

Identification of a fluorescent general anesthetic, 1-aminoanthracene

Christopher A. Butts^a, Jin Xi^b, Grace Brannigan^c, Abdalla A. Saad^d, Srinivasan P. Venkatachalan^d, Robert A. Pearce^d, Michael L. Klein^c, Roderic G. Eckenhoff^{b,1}, and Ivan J. Dmochowski^{a,1}

^aDepartment of Chemistry, University of Pennsylvania, 231 South 34th Street, Philadelphia, PA 19104; ^bDepartment of Anesthesiology and Critical Care, University of Pennsylvania School of Medicine, 311A John Morgan Building, 3620 Hamilton Walk, Philadelphia, PA 19104; ^cCenter for Molecular Modeling, University of Pennsylvania, 231 South 34th Street, Philadelphia, PA 19104; and ^dDepartments of Anesthesiology and Physiology, University of Wisconsin, 601 Science Drive, Madison, WI 53711

Edited by Elizabeth C. Theil, Children's Hospital Oakland Research Institute, Oakland, CA, and accepted by the Editorial Board March 4, 2009 (received for review October 21, 2008)

We identified a fluorophore, 1-aminoanthracene (1-AMA), that is anesthetic, potentiates GABAergic transmission, and gives an appropriate dissociation constant, $K_d \approx 0.1$ mM, for binding to the general anesthetic site in horse spleen apoferritin (HSAF). 1-AMA fluorescence is enhanced when bound to HSAF. Thus, displacement of 1-AMA from HSAF by other anesthetics attenuates the fluorescence signal and allows determination of K_d , as validated by isothermal titration calorimetry. This provides a unique fluorescence assay for compound screening and anesthetic discovery. Additional electrophysiology experiments in isolated cells indicate that 1-AMA potentiates chloride currents elicited by GABA, similar to many general anesthetics. Furthermore, 1-AMA reversibly immobilizes stage 45–50 *Xenopus laevis* tadpoles ($EC_{50} = 16 \mu\text{M}$) and fluorescence micrographs show 1-AMA localized to brain and olfactory regions. Thus, 1-AMA provides an unprecedented opportunity for studying general anesthetic distribution in vivo at the cellular and subcellular levels.

ferritin | probe | GABA | propofol | imaging

Despite controlled administration by trained physicians, current general anesthetics are still responsible for morbidity and mortality (1, 2). Reports are also emerging that durable cognitive effects may occur from anesthesia, in particular, in the elderly (3–5) and very young (6–8), and repeated exposure may hasten the onset of neurodegenerative disease (9–11). Several factors have slowed efforts to identify safer and more effective anesthetics, not least of which is the large number ($\approx 10^{60}$) of candidate molecules with molecular mass ≤ 500 g/mol (12). It is also problematic that the most relevant molecular targets of clinical anesthetics have not been definitively assigned, and their in vivo distribution is poorly understood. Fluorescent probes offer the potential to address these problems, with the caveat that tethering a fluorophore to the typically small anesthetic is likely to eliminate its activity. This motivated our search for an intrinsically fluorescent general anesthetic.

Common general anesthetics are thought to act on membrane receptor proteins such as ion channels (13), which are large, water insoluble, and difficult to obtain in pure form; they contain many interacting small-molecule binding sites. Thus, screening small-molecule libraries by using putative anesthetic receptors is not currently feasible. Recently, we identified a high-affinity general anesthetic binding site on a readily available, water-soluble protein, horse spleen apoferritin (HSAF) (14). HSAF is comprised of 24 four-helix bundle subunits that self-assemble to form a protein shell with 4,3,2-symmetry, which functions to sequester iron as ferric hydroxide (15, 16). Crystal structures of HSAF complexed with isoflurane or halothane show that the anesthetics bind in single $\approx 400 \text{ \AA}^3$ hydrophobic cavities formed at the interfaces between pairs of four-helix bundle subunits (14). Ferritin exhibits striking architectural similarities to the transmembrane region of the superfamily of ligand-gated channels, such as the GABA_A receptor, which is a pentamer of

4- α -helix bundles, with the proposed anesthetic site at the interhelical, subunit interface (Fig. 1) (17). The strength of small-molecule binding interactions with HSAF correlates well with anesthetic potency (supporting information (SI) Fig. S1). These features recommend HSAF as a potential model protein receptor for screening fluorescent probes and new drug candidates.

We identified the fluorophore 1-aminoanthracene (1-AMA) as a general anesthetic by searching for probe molecules that bind HSAF and compete with known anesthetics. 1-AMA is a polarity-sensitive hydrophobic probe that has been used previously to investigate different protein cavities (18–21). We report that 1-AMA shows enhanced fluorescence intensity at 515 nm when complexed with HSAF. Binding to the HSAF site of interest is indicated by a large decrease in 1-AMA fluorescence on addition of general anesthetics. This suggests that a fluorescence assay based on 1-AMA and HSAF should be useful for compound screening. Interestingly, 1-AMA has physicochemical properties similar to propofol, a common i.v. general anesthetic: They are similar in molecular mass (193 g/mol for 1-AMA vs. 178 g/mol for propofol), hydrophobicity as measured by \log_{10} of the octanol/water partition coefficient ($\log P = 3.7$ vs. 3.8), and polar surface area (26 cm² vs. 20 cm²) (22). Moreover, 1-AMA was found to potentiate GABA-induced chloride transport in isolated cells, induce reversible immobility in *Xenopus* tadpoles, and enable in vivo fluorescence imaging studies, which show localization in neuronal tissue.

Results

Measuring 1-AMA Binding to HSAF. We determined that small organic solubilizing agents such as MeOH compete with 1-AMA binding to HSAF, in agreement with previous 1-AMA studies (19). Thus, to 1-mL solutions of 1-AMA in 10% PEG-400 and PBS buffer (final concentration, 1–220 μM) was added 20 μL of HSAF (final concentration, 1.55 μM 24-mer, 18.6 μM dimer). Emission data were corrected for contributions from 1-AMA and HSAF alone in 10% PEG-400 and PBS buffer. A dissociation constant, $K_d = 70 \pm 20 \mu\text{M}$ (95% confidence limit) at 298 K, was determined for data points up to 220 μM 1-AMA by curve fitting to a single-site binding model (Fig. 2),

$$Y = \frac{B_{\max} \cdot X}{(K_d + X)} \quad [1]$$

Author contributions: R.A.P., M.L.K., R.G.E., and I.J.D. designed research; C.A.B., J.X., G.B., A.A.S., S.P.V., R.G.E., and I.J.D. performed research; C.A.B., R.A.P., R.G.E., and I.J.D. analyzed data; and C.A.B., R.G.E., and I.J.D. wrote the paper.

The authors declare no conflict of interest.

This article is a PNAS Direct Submission. E.C.T. is a guest editor invited by the Editorial Board.

¹To whom correspondence may be addressed. E-mail: roderic.eckenhoff@uphs.upenn.edu or ivandmo@sas.upenn.edu.

This article contains supporting information online at www.pnas.org/cgi/content/full/0810590106/DCSupplemental.

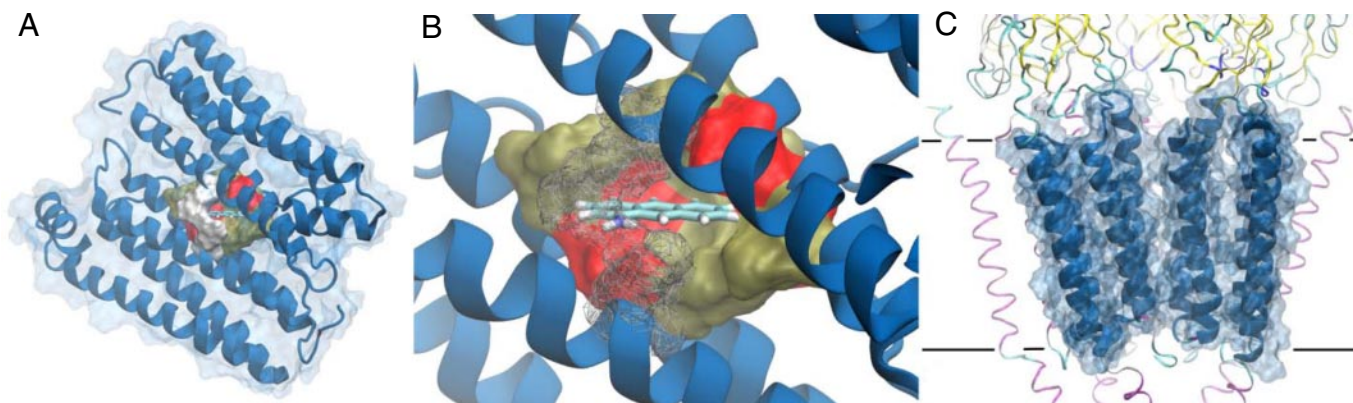


Fig. 1. Proposed binding site for 1-AMA. (A) Ferritin dimer composed of two 4-helix bundles (blue) with interfacial cavity residues shown in surface representation: polar (red), nonpolar (tan), and Arg-59 (white). (B) Conformation of cavity residues and 1-AMA after energy minimization: the ligand rotates from its initial docked position, and the two Arg-59 residues (now in white wire frame) arc away from the cavity to accommodate the ligand amino group. Other cavity residues are largely unaffected by ligand binding. (C) The 4-helix bundle motif is also found in the transmembrane domains of anesthetic-sensitive Cys loop receptor subunits. The nicotinic acetylcholine receptor (PDB ID code 2BG9) (36) is shown with the transmembrane domains of 2 of the 5 subunits highlighted in blue; the interface between the subunits contains numerous gaps in protein density that could offer potential anesthetic binding sites. Horizontal lines indicate the membrane-water interface.

where Y is the corrected fluorescence intensity, B_{\max} is the maximal Y value, X is [1-AMA], and K_d is the concentration of [1-AMA] required to reach half-maximal binding. Because the K_d exceeds the maximum water solubility of 1-AMA ($\approx 33 \mu\text{M}$), it should be viewed as an estimate.

Isothermal titration calorimetry (ITC) was performed to validate the fluorescence results and obtain thermodynamic parameters for 1-AMA binding to the HSAF dimer ($\Delta H = 3.3 \pm 0.1 \text{ kcal mol}^{-1}$; $\Delta S = -7.1 \text{ cal mol}^{-1} \text{ K}^{-1}$). Because of 1-AMA's limited water solubility, a reverse titration was performed, whereby 0.67 mM HSAF in 10% PEG-400 in PBS was titrated into an ITC cell containing a saturated solution of 1-AMA in the same PEG-containing buffer. ITC provided a dissociation constant for the HSAF-1-AMA complex ($K_d = 96 \pm 11 \mu\text{M}$ at 298 K; Fig. 3), which was in good agreement with the fluorescence data and confirmed 1-AMA binding. As seen in Figs. 2 and 3, modest solubility of 1-AMA in 10% PEG-400 and PBS buffer prevented complete saturation of HSAF binding sites.

Evidence of 1-AMA occupation of the HSAF anesthetic site, instead of an allosterically coupled remote site, comes from molecular docking and energy minimization approaches show-

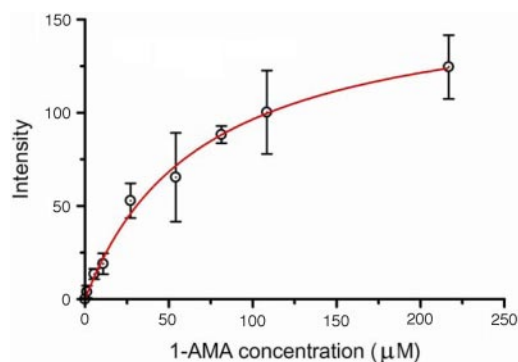


Fig. 2. Fluorescence assay measuring binding of 1-AMA to HSAF. To a 1-mL solution of 1-AMA (1 μM –1.25 mM) in 10% PEG-400/PBS, pH 7, was added 20 μL of 38 mg/mL HSAF (final [HSAF dimer] = 18.6 μM). Samples were excited at 380 nm and fluorescence monitored at 515 nm. Intensities from “bound” 1-AMA were obtained by subtracting contributions from HSAF and unbound 1-AMA. All trials were run in triplicate at 298 K. Data and error analysis was carried out by using Prism4.0 (GraphPad Software, Inc.).

ing 1-AMA binding without significant distortion or steric clash at the anesthetic site (Fig. 1). During energy minimization, 1-AMA rotated in the HSAF anesthetic cavity, which was accommodated by adjustment of both Arg-59 residues at the 2-fold symmetric interface. The conformation of these Arg-59 residues at the cavity mouth has previously been shown to be

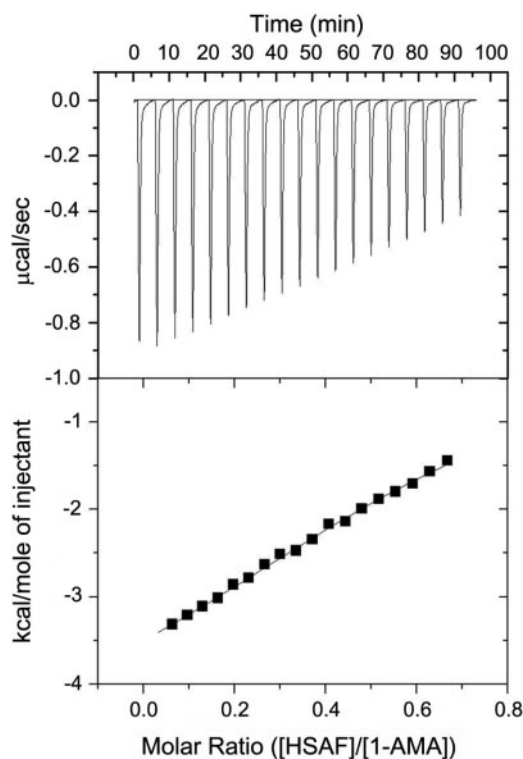


Fig. 3. Isotherm of HSAF titration into 1-AMA. HSAF (0.67 mM) in 10% PEG-400 and PBS, pH 7, was loaded into the ITC syringe (0.286 mL), and 1-AMA (0.22 mM) in the same 10% PEG solution was loaded into the cell (1.43 mL). Titrations were performed at 298 K by using a VP ITC (Microcal). (Upper) Raw heat data ($\mu\text{cal/s}$) versus time (min). (Lower) Normalized integrated data (kcal/mol HSAF vs. molar ratio, [HSAF]/[1-AMA]). Origin 5.0 (Microcal Software) was used to fit thermodynamic parameters for a single-class-binding model to the heat profiles.

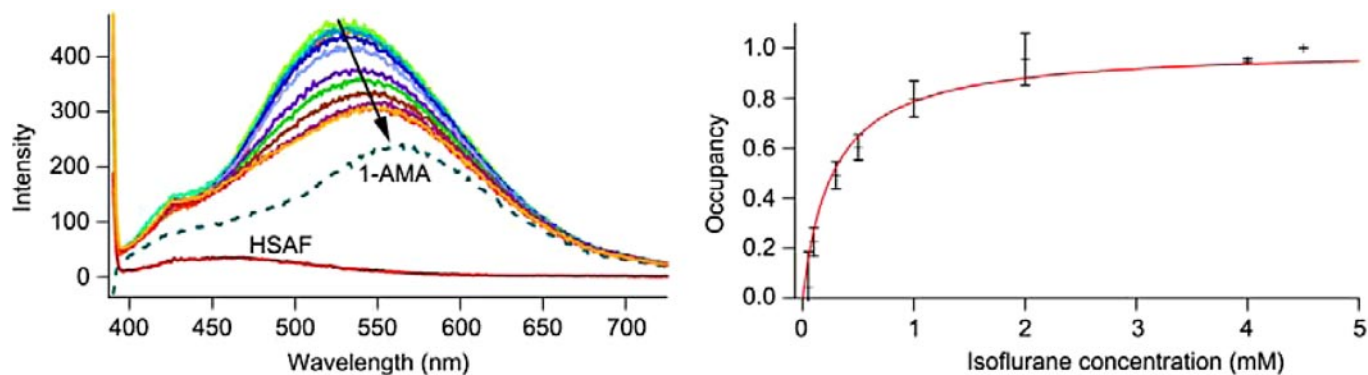


Fig. 4. Determination of isoflurane binding to HSAF through 1-AMA displacement. (Left) Fluorescence spectra after addition of 1 μM to 4.5 mM isoflurane to HSAF (313 nM) preequilibrated with 10.5 μM 1-AMA. Samples excited at 380 nm. Downward arrow indicates AMA displacement on isoflurane titration. Dashed line indicates 1-AMA alone in solution. HSAF (bottom spectrum) contributes little to fluorescence at 520 nm. (Right) Plot of isoflurane occupancy vs. isoflurane concentration after displacement of 1-AMA from HSAF. Error bars indicate standard error of data points from titrations performed in triplicate. Curve fitting (red line) was performed in Igor Pro 4.01 (Wave Metrics).

sensitive to occupancy of this cavity (14). Although the effective cavity size may consequently be larger when occupied by 1-AMA than with halothane, all residues besides Arg-59 remained virtually stationary.

Measuring Isoflurane and Propofol Binding to HSAF by 1-AMA Displacement. To further confirm binding at the anesthetic site on HSAF, a competition assay was performed by using isoflurane, a clinical anesthetic that has been confirmed crystallographically to bind at the HSAF anesthetic site (14). As isoflurane was titrated, the fluorescence signal from 1-AMA (Fig. 4 Left) decreased in a manner well fit by a single-site binding model (Eq. 1, Fig. 4 Right). Curve fitting to the Hill equation identified an IC_{50} for isoflurane of 270 $\mu\text{M} \pm 30 \mu\text{M}$ at 298 K, which was corrected by using the Cheng-Prusoff equation,

$$K_{d,\text{true}} = \text{EC}_{50} \cdot \frac{1}{1 + \left(\frac{1}{K_{d,1\text{-AMA}}} \cdot [1\text{-AMA}] \right)} \quad [2]$$

to yield a K_d of 235 μM (20). This is comparable to the value determined for isoflurane by direct measurement by using ITC and assuming a single class of sites (14). These data provide strong evidence that 1-AMA also binds to the HSAF anesthetic site.

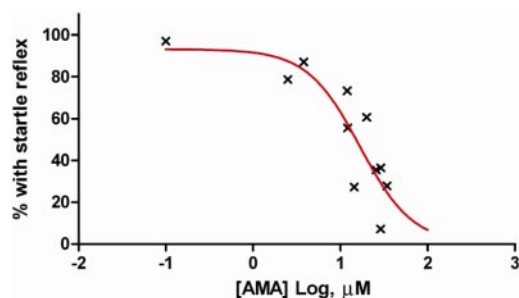


Fig. 5. Anesthetic potency of 1-AMA in *Xenopus* tadpoles determined from measuring startle response according to the procedure of Xi et al. (37). Tadpoles ($n = 10\text{--}15$) incubated in pond water for 1 h were tested at several different concentrations of 1-AMA (1–33 μM), with the final concentration determined by UV-visible (UV-vis) spectroscopy. The startle response was measured by sharply tapping on the top of each dish with a wooden applicator, averaged over 3 taps. Percent responses vs. concentration data were fitted to variable slope Hill curves by using GraphPad Prism4.0.

We subsequently investigated the use of the 1-AMA/HSAF competition assay in a higher-throughput, 96-well plate format. Propofol is an oily GABAergic general anesthetic with only moderate volatility, which makes it possible to control concentrations in an open system. Propofol displaced 1-AMA with an IC_{50} of 11 μM (95% CI = 7–17 μM) and Hill slope of -0.8 (95% CI = -1.1 to -0.6) (Fig. S2). The calculated K_d of 10 μM (Eq. 2) is similar that obtained by ITC, and is a reasonable approximation of the EC_{50} observed to enhance GABA_A currents and produce anesthesia in vivo (13). This provides further validation of the GABA_A mimicry by the apoferritin site, and demonstrates the utility of 1-AMA to study compound binding to the HSAF anesthetic site.

Anesthetic Functional Assays. Having validated 1-AMA from HSAF binding studies and competition assays as a likely anesthetic candidate, the anesthetic potency of 1-AMA was verified in *Xenopus* tadpoles by measuring the startle reflex. At the highest concentration achievable in pond water ($\approx 33 \mu\text{M}$), almost all animals lost their startle reflex within 15–20 min (Fig. 5). Based on this assay, the EC_{50} for 1-AMA was 16 μM (95% C.I. = 8–34 μM), and Hill slope of 1.4 (95% C.I. = 0.1–3.0). Most tadpoles recovered fully but slowly from the immobilized state when returned to pure pond water. However, $\approx 50\%$ of the tadpoles that had been exposed to the highest 1-AMA concentrations subsequently died over a period of hours, most likely due to toxic metabolites of 1-AMA (23).

Most general anesthetics in use today are positive modulators of GABA_A receptors—i.e., they enhance responses to application of their naturally occurring agonist, γ -aminobutyric acid (GABA). Fig. 6 clearly shows that 1-AMA shares this feature in a heterologous expression system. Consistent with the observation that 1-AMA solubility is lower than its HSAF K_d , and therefore probably the GABA_A receptor K_d as well, there was no evidence of saturation of receptor potentiation at concentrations up to 30 μM 1-AMA.

1-AMA in Vivo Fluorescence Imaging. Albino tadpoles immobilized with 1-AMA ($\approx 33 \mu\text{M}$) were imaged by using confocal laser scanning microscopy to determine anesthetic distribution in vivo, as well as subcellular localization. Whereas the few volatile general anesthetics in current clinical use that have been studied (i.e., halothane, sevoflurane) are promiscuous and distribute broadly (24), 1-AMA was observed to localize primarily in *Xenopus* neuronal tissue (Fig. 7), with weak fluorescence also observed in the heart (Fig. S3) and other organs. These in vivo fluorescence

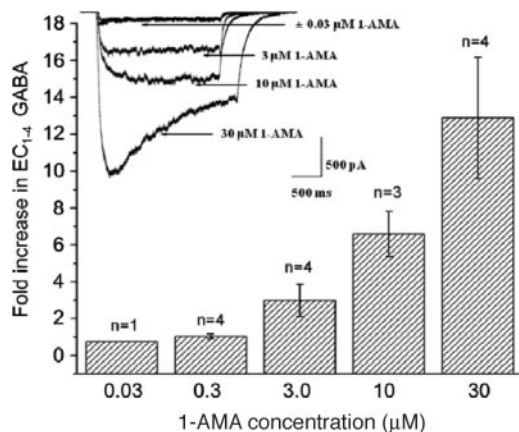


Fig. 6. Fold change of chloride current in the presence of 4 μM GABA and 1-AMA at the shown concentrations normalized to the effect of 4 μM GABA alone. Each bar represents recordings from n cells. (Inset) Measurement of chloride current with 4 μM GABA and varying concentrations of 1-AMA (0–30 μM).

intensities are readily assigned to 1-AMA, as opposed to cellular autofluorescence. Fluorescence was observed immediately and did not vary during imaging, which discounts contributions from 1-AMA metabolites. The *in vivo* fluorescence spectrum (broad emission peak with maximum ≈ 520 nm) matches that of 1-AMA in a low dielectric environment. Moreover, images taken by using the same confocal microscope settings on *Xenopus* immobilized with propofol show no fluorescence signal (Fig. S4). High-resolution confocal optical sections taken with a 40 \times objective lens show the subcellular localization of 1-AMA within a neuron in the tadpole brain (Fig. 8). 1-AMA is localized to the nucleus broadly distributed within the neuron, whereas it appears more faintly at the nuclear membranes in the adjoining cells.

Discussion

The isoflurane and propofol competition studies, as well as 1-AMA modeling data presented herein strongly indicate that 1-AMA binds in the anesthetic site. Moreover, displacement of 1-AMA by propofol supports the GABA_A mimicry of HSAF. These data suggest the use of this 1-AMA/HSAF assay for screening new compounds, which should allow a more complete

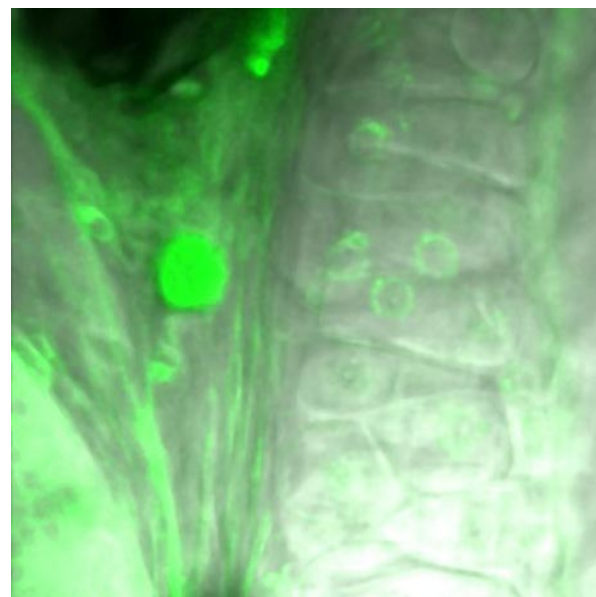


Fig. 8. Confocal micrograph of a neuronal cell (left of image) within the brain of an albino stage 45–50 *X. laevis* tadpole immobilized with 33 μM 1-AMA for 1 h in pond water. This higher magnification image shows subcellular localization of 1-AMA (green fluorescence overlaid on transmitted light image).

investigation of steric and electronic factors that contribute to drug binding, while correlating the strength of these interactions with anesthetic potency.

Fluorescence-based binding assays offer large advantages in speed and sensitivity over methods such as isothermal titration calorimetry. One limitation has been that many common fluorophores incorporate substituted aromatic moieties and have molecular volumes exceeding the volume of the HSAF anesthetic site. Similar volume limitations are known to be relevant for genuine anesthetic targets, because clinical anesthetic potency falls off dramatically at molecular masses >180 g/mol (i.e., dodecanol in the *n*-alkanol series) (25). This is consistent with initial experiments with the fluorophore ANS (molecular mass = 299 g/mol), which showed no change in fluorescence signal on the addition of HSAF, likely because of its large size.

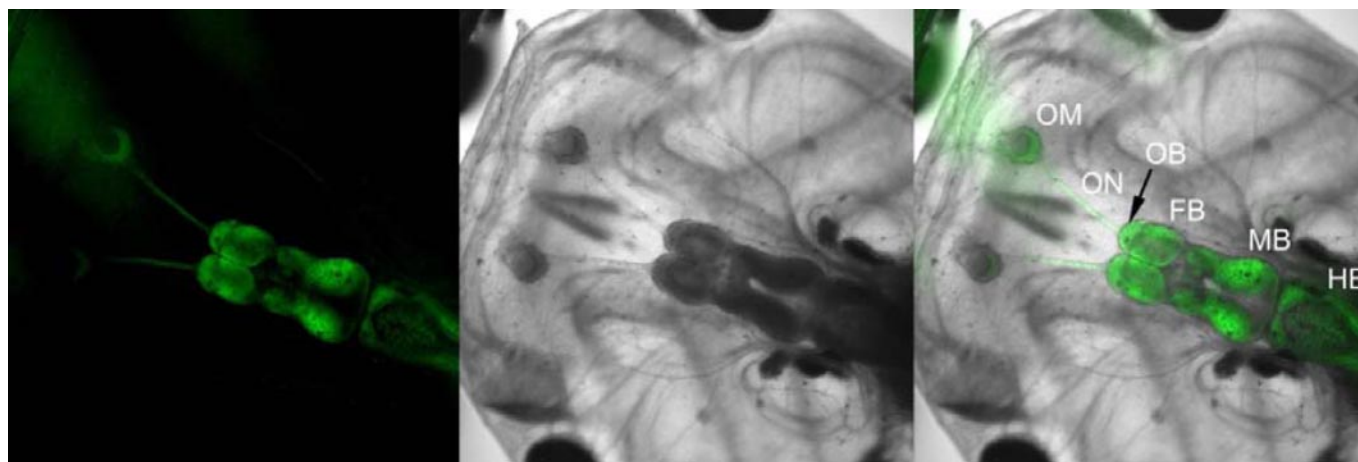


Fig. 7. Confocal micrographs of albino stage 45–50 *Xenopus laevis* tadpoles immobilized with 33 μM 1-AMA for 1 h in pond water. Images of *Xenopus* head show 1-AMA localization within the brain, spinal cord, and olfactory system. (Left) Fluorescence image. (Center) Transmitted light image. (Right) Overlay, with labeled olfactory mucosa (OM), olfactory neuron (ON), olfactory bulb (OB), forebrain (FB), midbrain (MB), and hindbrain (HB). Sample was excited at 488 nm and emission collected from 515 to 550 nm.

By comparison, 1-AMA shows great promise as an HSAF binder and anesthetic probe molecule, based on its solvachromatic properties and modest molecular size.

The GABA enhancement observed at 30 μM 1-AMA was large (≈ 13 -fold), suggesting a robust GABAergic effect at 1-AMA's solubility limit, and consistent with the *in vivo* EC_{50} being somewhat below this concentration. Thus, 1-AMA shares *in vitro* features of many contemporary general anesthetics, such as propofol (26), lending further credibility to the use of an HSAF/1-AMA assay for compound screening and discovery.

Given this GABAergic character, the localization of 1-AMA to neuronal tissue is best explained by selectivity to the ligand-gated ion channel superfamily, although other neuronal targets, such as G protein-coupled receptors (20, 26) cannot be ruled out. The distribution within the tadpole head seems inconsistent with simple lipid distribution, because it would have been expected to distribute much more broadly. This provides additional support for the notion that specific neuronal proteins are the direct targets for general anesthetics.

Interestingly, confocal micrographs of the tadpole brain (Fig. 7) show nonuniform 1-AMA fluorescence intensity, which is likely due to the variable distribution of specific and nonspecific anesthetic sites within the brain. Localization in the cerebral lobe of the brain might arise because of the high density of synaptic contacts and associated signaling systems (27). This finding agrees with previous studies of the rat brain, in which regions with high concentrations of anesthetic were correlated with high synaptic density (gray matter) (28) and unidentified macromolecular receptors (29). By using standard confocal laser scanning microscopy imaging systems and light sources, it should be possible to use 1-AMA for understanding the distribution and modulation of anesthetic targets. At the excitation wavelength (488 nm) at which most of the present confocal imaging studies in tadpoles were conducted, 1-AMA has trace absorbance (Fig. S5) but still provides ample fluorescence signal either in a cuvette (in PEG-400, Fig. S6) or *in vivo* by using intermediate confocal PMT voltage settings. Excitation near an absorbance maximum of 1-AMA (≈ 380 nm) can enhance fluorescence signals, but also reduces depth penetration and increases background autofluorescence. For optical imaging of 1-AMA in larger animals, 2-photon microscopy may offer some advantages.

The lack of 1-AMA fluorescence from many parts of the tadpole suggests that ferritin itself contributes little to the distribution of the observed signal. Ferritin has been identified in all animal tissues, with highest concentrations usually found in liver, spleen, and bone marrow (30). Although iron is an important element for the central nervous system, excessive brain iron is neurotoxic, and via Fenton chemistry produces free radicals that can cause oxidative damage of different cellular components. This may explain why ferritin concentrations in the healthy brain are typically low (31).

Biological ferritin sequesters iron as a ferric oxide mineral core, which has little effect on 1-AMA binding but appears to quench approximately half of the fluorescence intensity (Fig. S7), likely by an electron-transfer process. Moreover, 488-nm excitation of 1-AMA bound to horse spleen ferritin (HSF) or HSAF in a cuvette produces only a weak fluorescent signal ≈ 520 nm (Fig. S8). Thus, ferritin is expected to contribute very little to the 1-AMA fluorescence observed in the tadpole brain.

Previous efforts to image the distribution of clinical anesthetics in laboratory animals made use of signals from the available carbon and halogen atoms. For example, ^{14}C -halothane was quantified by autoradiography in fixed sections of the rat brain,

where the volatile anesthetic was immobilized by photolabeling (28) or sample freezing (32, 33). And, the distribution of sevoflurane in the head of a live rat was measured by ^{19}F NMR imaging (29). Fluorescence imaging is a very sensitive and rapid technique, and provides much better spatiotemporal resolution than can be achieved by using autoradiography or NMR. As a demonstration, the confocal micrographs of 1-AMA in a tadpole represent the first high-resolution images of a general anesthetic distribution in an immobilized, living animal. Moreover, as shown in Fig. 8, it is possible to obtain much higher resolution images of 1-AMA in neurons within the brain of the living tadpole. This image raises interesting questions about the interactions of 1-AMA with the cellular and nuclear membranes, and other membranes within the cell, where anesthetics are proposed to bind GABA_A and other ligand-gated receptors.

In summary, 1-AMA binds to a site on HSAF ($K_d \approx 0.1$ mM) with comparable affinity as other known anesthetic molecules, and provides a useful measure of unknown compound binding through competition assays. We found that 1-AMA is a fluorescent, GABAergic general anesthetic, which provides avenues for imaging anesthetic activity with unprecedented spatial and temporal resolution. The favorable fluorescence properties of 1-AMA coupled with HSAF's high level of structural mimicry of relevant regions of ligand-gated ion channels, aqueous solubility, ready availability, and ease of crystallization and structure determination, make this combination an ideal high-throughput system for the determination of potentially new classes of anesthetic molecules.

Methods

See *SI Text* for detailed methods and data.

Molecular Docking of 1-AMA. A likely orientation for 1-AMA in the HSAF cavity was determined by manually docking 1-AMA into the cavity by using VMD (34), and then energy minimizing the ligand and protein side chains according to the CHARMM-22 force field (35). The initial coordinates for the HSAF 4-helix bundle subunit were taken from the X-ray structure in the presence of halothane (PDB ID code 1XZ1) (14).

UV-Vis Spectroscopy. All UV-Vis measurements were made with an Agilent Technologies 8453 spectrophotometer with 89090A temperature controller and magnetic stirrer, using a quartz cuvette with 1-cm pathlength. 1-AMA stock solutions were made by using $\epsilon_{368} = 4,240 \text{ M}^{-1} \text{ cm}^{-1}$. The concentration of pure HSAF 24-mer was determined by both Bradford assay and UV-Vis spectroscopy.

Fluorescence Spectroscopy. 1-AMA was excited at 380 nm and fluorescence data were collected from 390 to 720 nm by using a Cary Eclipse fluorescence spectrophotometer (Varian) and the Cary Eclipse Bio software package.

GABA_A Electrophysiological Recordings. Cells were cultured and transfected as described in *SI Text*. Recordings were performed at room temperature on the stage of a Leica inverted microscope. Solutions were applied to lifted whole-cells by using a custom-designed 12-barrel application system. An open-tip solution exchange time constant (τ) of 20–30 ms was typically achieved. The recording chamber was perfused continuously with HEPES-buffered saline. GABA solutions were diluted to the desired concentration (4 μM) in this same control/bath solution. 1-AMA solutions were added in the same buffer, at the concentrations shown in Fig. 6.

ACKNOWLEDGMENTS. We thank Dr. Jeffery Saven for use of the fluorimeter. This work was supported by National Science Foundation Grant CHE-0548188, National Center for Research Resources Award 1S10-RR-021113-01, a Henry and Camille Dreyfus Teacher-Scholar award (to I.J.D.), National Institutes of Health Grants GM51595 and GM55876 (to R.G.E.), and National Institutes of Health Grants GM47818 and NS056411 (to R.A.P.). This collaborative effort was initiated with an University of Pennsylvania Institute for Medicine and Engineering Seed Grant (to I.J.D. and R.G.E.).

1. Eagle CC, Davis NJ (1997) Report of the anaesthetic mortality committee of Western Australia 1990–1995. *Anaesth Intensive Care* 25:51–59.
2. Warden JC, Horan BF (1996) Deaths attributed to anaesthesia in New South Wales, 1984–1990. *Anaesth Intensive Care* 24:66–73.

3. Dodds C, Allison J (1998) Postoperative cognitive deficit in the elderly surgical patient. *Br J Anaesth* 81:449–462.
4. Moller JT, et al. (1998) Long-term postoperative cognitive dysfunction in the elderly: ISPOCD1 study. *Lancet* 351:857–861.

5. Parikh SS, Chung F (1995) Postoperative delirium in the elderly. *Anesth Analg* 80:1223–1332.
6. Anand KJS (2007) Anesthetic neurotoxicity in newborns: Should we change clinical practice? *Anesthesiology* 107:2–4.
7. Jevtovic-Todorovic V, et al. (2003) Early exposure to common anesthetic agents causes widespread neurodegeneration in the developing rat brain and persistent learning deficits. *J Neurosci* 23:876–882.
8. Ikonomidou C, et al. (1999) Blockade of NMDA receptors and apoptotic neurodegeneration in the developing brain. *Science* 283:70–74.
9. Bohnen N, Warner MA, Kokmen E, Kurland LT (1994) Early and midlife exposure to anesthesia and age of onset of Alzheimer's disease. *Int J Neurosci* 77:181–185.
10. Eckenhoff RG, et al. (2004) Inhaled anesthetic enhancement of amyloid- β oligomerization and cytotoxicity. *Anesthesiology* 101:703–709.
11. Xie Z, et al. (2007) The inhalation anesthetic isoflurane induces a vicious cycle of apoptosis and amyloid beta-protein accumulation. *J Neurosci* 27:1247–1254.
12. Bohacek RS, McMartin C, Guida WC (1996) The art and practice of structure-based drug design: A molecular modeling perspective. *Med Res Rev* 16:3–50.
13. Campagna JA, Miller KW, Forman SA (2003) Mechanisms of actions of inhaled anesthetics. *The New England Journal of Medicine* 348:2110–2124.
14. Liu R, Loll PJ, Eckenhoff RG (2005) Structural basis for high-affinity volatile anesthetic binding in a natural 4-helix bundle protein. *FASEB J* 19:567–576.
15. Hempstead PD, et al. (1997) Comparison of the three-dimensional structures of recombinant human H and horse L ferritins at high resolution. *J Mol Biol* 268:424–448.
16. Theil EC (2001) *Handbook of Metalloproteins*, eds Messerschmidt A, Huber R, Poulos T, Wieghardt K (John Wiley & Sons, Chichester, U.K.), pp 771–781.
17. Li G-D, et al. (2006) Identification of a GABA_A receptor anesthetic binding site at subunit interfaces by photolabeling with an etomidate analog. *J Neurosci* 26:11599–11605.
18. Paolini S, Tanfani F, Fini C, Bertoli E, Pelosi P (1999) Porcine odorant binding protein: Structural stability and ligand affinities measured by fourier-transform infrared spectroscopy and fluorescence spectroscopy. *Biochim Biophys Acta* 1431:179–188.
19. Vincent F, et al. (2004) Crystal structures of bovine odorant-binding protein in complex with odorant molecules. *Eur J Biochem* 271:3832–3842.
20. Johansson JS, Manderson GA, Ramoni R, Grolli S, Eckenhoff RG (2005) Binding of the volatile general anesthetics halothane and isoflurane to a mammalian β -barrel protein. *FEBS J* 272:573–581.
21. Paliwal A, De PK (2007) Purification, cloning and regulation of a novel acid-lipase-like protein of hamster expressed in lacrimal glands and tears during lactation. *Biochim Biophys Acta* 1771:55–65.
22. Torres-Cartas S, Martín-Biosca Y, Villanueva-Camañasa RM, Sagrado S, Medina-Hernández MJ (2007) Biopartitioning micellar chromatography to predict mutagenicity of aromatic amines. *Eur J Med Chem* 42:1396–1402.
23. Zhan J, Gunatilaka AA (2008) Microbial metabolism of 1-aminoanthracene by *Beauveria bassiana*. *Bioorg Med Chem* 16:5085–5089.
24. Eckenhoff RG (2001) Promiscuous ligands and attractive cavities. *Mol Interventions* 1:258–268.
25. Alifimoff JK, Firestone LL, Miller KW (1989) Anaesthetic potencies of primary alkanols: Implications for the molecular dimensions of the anaesthetic site. *Br J Pharmacol* 96:9–16.
26. Belelli D, Pistis M, Peters JA, Lambert JJ (1999) The interaction of general anaesthetics and neurosteroids with GABA_A and glycine receptors. *Neurochem Int* 34:447–452.
27. Kandel ER, Schwartz JH, Jessell TM (2000) *Principles of Neural Science* (McGraw-Hill, New York), 4th Ed.
28. Eckenhoff MF, Eckenhoff RG (1998) Quantitative autoradiography of halothane binding in rat brain. *J Pharmacol Exp Ther* 285:371–376.
29. Xu Y, Tang P, Zhang W, Firestone L, Winter PM (1995) Fluorine-19 nuclear magnetic resonance imaging and spectroscopy of sevoflurane uptake, distribution, and elimination in rat brain. *Anesthesiology* 83:766–774.
30. Munro HN, Linder MC (1978) Ferritin: Structure, biosynthesis, and role in iron metabolism. *Physiol Rev* 58:317–396.
31. Snyder AM, Connor JR (2008) Iron, the substantia nigra and related neurological disorders. *Biochim Biophys Acta*, 10.1016/j.bbagen.2008.08.005.
32. Cohen EN, Chow KL, Mathers L (1972) Autoradiographic distribution of volatile anesthetics within the brain. *Anesthesiology* 37:324–330.
33. Cohen EN, Hood N (1969) Application of low temperature autoradiography to studies of the uptake and metabolism of volatile anesthetics in the mouse. 3. Halothane. *Anesthesiology* 31:553–559.
34. Humphrey VV, Dalke A, Schulten K (1996) VMD: Visual molecular dynamics. *J Mol Graph* 14:33–38-27–38.
35. MacKerell A, et al. (1998) All-atom empirical potential for molecular modeling and dynamics studies of proteins. *J Phys Chem B* 102:3586–3616.
36. Unwin N (2005) Refined structure of the nicotinic acetylcholine receptor at 4 Å resolution. *J Mol Biol* 346:967–989.
37. Xi J, et al. (2006) Photoactive analogues of the haloether anesthetics provide high-resolution features from low-affinity interactions. *ACS Chem Biol* 1:377–384.